ACS APPLIED MATERIALS & INTERFACES

Research Article

www.acsami.org

Facile Synthesis of Gd–Cu–In–S/ZnS Bimodal Quantum Dots with Optimized Properties for Tumor Targeted Fluorescence/MR *In Vivo* Imaging

Weitao Yang,[†] Weisheng Guo,[§] Xiaoqun Gong,[†] Bingbo Zhang,[*,‡] Sheng Wang,[†] Na Chen,[∥] Wentao Yang,[†] Yu Tu,[∥] Xiangming Fang,[⊥] and Jin Chang[*,†]

[†]School of Materials Science and Engineering, School of Life Science, Tianjin Engineering Center of Micro-Nano Biomaterials and Detection-Treatment Technology, Collaborative Innovation Center of Chemical Science and Engineering, Tianjin University, Tianjin 300072, China

[‡]Shanghai East Hospital, The Institute for Biomedical Engineering & Nano Science, Tongji University School of Medicine, Shanghai 200092, China

[§]CAS Key Laboratory for Biological Effects of Nanomaterials & Nanosafety, National Center for Nanoscience and Technology, No. 11 Beiyitiao, Zhongguancun, Beijing 100190, China

[∥]Department of Medical Radioprotection, School of Radiation Medicine and Health, Soochow University, Suzhou 200072, China

[⊥]Department of Radiology, Wuxi People's Hospital Affiliated to Nanjing Medical University, Jiangsu 214023, China

Supporting Information

ABSTRACT: Dual-modal imaging techniques have gained intense attention for their potential role in the dawning era of tumor early accurate diagnosis. Chelate-free robust dual-modal imaging nanoprobes with high efficiency and low toxicity are of essential importance for tumor targeted dual-modal *in vivo* imaging. It is still a crucial issue to endow Cd-free dual-modal nanoprobes with bright fluorescence as well as high relaxivity. Herein, a facile synthetic strategy was developed to prepare Gd-doped CuInS/ZnS bimodal quantum dots (GCIS/ZnS, BQDs) with optimized properties. The fluorescent properties of the GCIS/ZnS BQDs can be thoroughly optimized by varying reaction temperature, aging time, and ZnS coating. The amount of Gd precursor can be well-controlled to realize the optimized balance between the MR relaxivity and optical properties. The obtained hydrophobic GCIS/ZnS BQDs were surface engineered into aqueous phase with PEGylated dextran-stearyl acid polymeric lipid vesicles (PEG-DS PLVs). Upon the phase transfer, the hydrophilic GCIS/ZnS@PLVs exhibited pronounced near-infrared fluorescence as well as high longitudinal relaxivity (r_1 = 9.45 mM^{-1} S^{-1}) in water with good colloidal stability. *In vivo* tumor-bearing animal experiments further verified GCIS/ZnS@PLVs could achieve tumor-targeted MR/fluorescence dual-modal imaging. No toxicity was observed in the *in vivo* and *ex vivo* experiments. The GCIS/ZnS@PLVs present great potential as bimodal imaging contrast agents for tumor diagnosis.

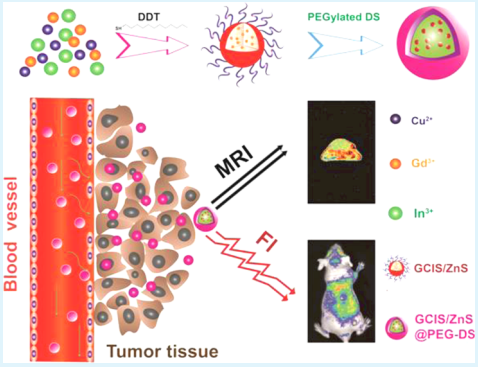

KEYWORDS: *quantum dots, MRI, targeted imaging, dual-modal imaging, fluorescence imaging*

1. INTRODUCTION

Current biomedical imaging techniques including MR, PET, CT, and ultrasound are playing vital roles in the diagnosis of various diseases. It is always a tough conundrum of modality selection in clinical diagnostic imaging that modalities with the highest sensitivity suffer relatively poor resolution, while those with higher resolution have relatively poor sensitivity. Recently, utilizing multiple modalities in combination has gained in popularity and facilitated harnessing the complementary abilities of different imaging modalities in tandem. As a typical example, MR/fluorescence dual-modal imaging has been of particular interest due to the following: (1) MR imaging can present the 3-D whole body images with high resolution but low sensitivity.[1−4] (2) Fluorescence imaging can provide functional information with high sensitivity but poor spatial resolution.[5,6] Consequently, in order to achieve accurate tumor diagnosis, versatile MR/fluorescence nanoprobes are also urgently needed to be established as dual-modal imaging contrast agents to enhance the MR/fluorescence imaging performance.

MR/fluorescence nanoprobes generally consist of fluorescent module and paramagnetic modules. Quantum dots (QDs) are considered to be promising candidates as the fluorescent module for biomedical applications,[7] which is due to their high

Received: June 17, 2015
Accepted: August 8, 2015
Published: August 8, 2015

DOI: 10.1021/acsami.5b05372
ACS Appl. Mater. Interfaces 2015, 7, 18759−18768

fluorescence quantum yields (QYs) and excellent photostability against photobleaching.[8,9] Paramagnetic ions (Mn and Gd) and iron oxide nanoparticles have been selected as paramagnetic modules to achieve MR enhancement. Accordingly, various kinds of MR/fluorescence nanoprobes have been successfully designed via three strategies:[10] bond conjugation, carrier encapsulation, and ion doping. Particularly, fluorescence/MR nanoprobes prepared by doping of QDs (CdSe, ZnO, and CdTe) with paramagnetic ions (Mn and Gd) have been adapted as elegant candidates for MRI/fluorescence dual-modal imaging, due to the ultrasmall size (<5 nm)[11,12] and robust structural stability. Wang et al. synthesized a series of Mn-doped II−VI CdSe/ZnS QDs by capping CdSe cores with paramagnetically doped ZnS shells.[13] Zhang et al. developed Gd-doped CdTe QDs as a dual-modality imaging agent for fluorescence/MR by a facile, one-pot, aqueous synthesis approach.[14] Lu et al. reported a simple and versatile method to develop MR/fluorescence nanoprobes by doping Gd in low toxic ZnO QDs.[10] Nevertheless, GdCuInS QDs should be ideal alternates to establish MR/fluorescence nanoprobes for *in vivo* imaging,[15] benefiting from their low toxicity and near-infrared fluorescence.[16,17] Additionally, the formed single crystal can enhance the structural stability and increase the surface utilization rate of nanoprobes. Therefore, inspired by the above development and issues, we set out to prepare reliable Gd-doped CuInS bimodal QDs for tumor targeted MR/fluorescence dual-modal *in vivo* imaging.

In this study, on the basis of our previous work on bimodal QDs,[18−21] we developed a facile synthesis of Gd-doped CuInS/ZnS BQDs (GCIS/ZnS) with optimized fluorescence/MR properties (Scheme 1). In this strategy, 1-dodecanethiol (DDT) was employed as the sulfur source and the only solvent, thus enabling green synthesis.[22,23] The cationic/anionic ratio can be well-controlled to optimize the combined MR/fluorescence properties of the GCIS/ZnS BQDs.[24] The obtained GCIS/ZnS BQDs present higher longitudinal relaxivity (r_1 = 9.4 mM^{-1} S^{-1}) than Magnevist (r_1 = 3.56 mM^{-1} S^{-1}), while the PL QYs of GCIS/ZnS BQDs can be as high as 50%. Animal experiments revealed that significant tumor targeted contrast enhancement could be observed by both MR and NIR fluorescence imaging, indicating the promise of GCIS/ZnS BQDs for great potential applications in biological and medical fields.

Scheme 1. Schematic Illustration of the Synthesis and Surface Modification of Gd-Doped CuInS/ZnS (GCIS/ZnS) BQDs Used for Dual-Modal (Fluorescence/MR) Imaging

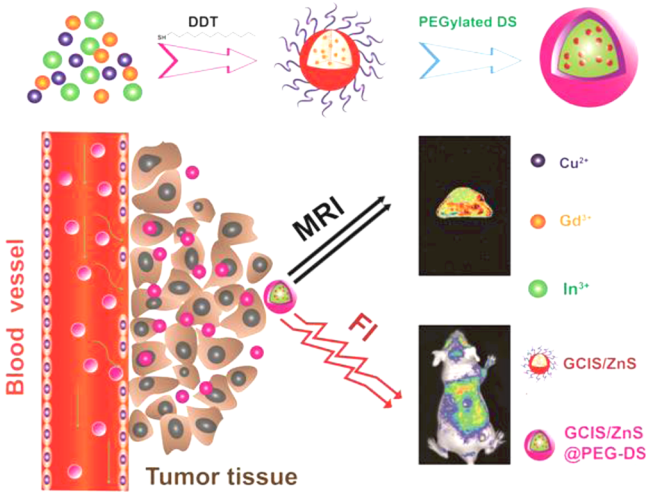

2. EXPERIMENTAL SECTION

2.1. Materials. Copper(III) acetylacetonate ($Cu(acac)_2$), zinc acetate dehydrate ($Zn(OAc)_2$, ACS, 98%), indium(III) 2,4-pentanedionate ($In(acac)_3$), gadolinium(III) 2,4-pentanedionate hydrate ($Gd(acac)_3{\cdot}xH_2O$), 1-dodecanethiol (DDT, 98%), 1-octadecene (ODE, 90%), oleic acid (OA, 90%), oleylamine (OLA, 70%), stearyl acid (SA), PEG-COOH (M_n = 2000), and 4-(dimethylamino)pyridine (DMAP) were obtained from Alfa Aesar China Co. Ltd. Dextran (M_w = 10 000) was purchased from Nanjing Duly Biotech Co., Ltd. (Jiangsu, China). *N*-(3-(Dimethylamino)propyl)-*N*-ethylcarbodiimide hydrochloride (EDC·HCl) was ordered from GL Biochem Ltd. (Shanghai, China). All chemicals were used without further purification. Deionized water (18.2 MΩ cm resistivity at 25 °C) was used throughout the entire experiments.

2.2. Synthesis of GCIS BQDs. GCIS BQDs with an average size of 3 nm were synthesized according to a modified procedure reported previously.[25] Typically, $Cu(acac)_2$ (0.2 mmol), $In(acac)_3$ (0.2 mmol), $Gd(acac)_3{\cdot}xH_2O$ (0.1 mmol), and DDT (15 mL) were mixed in the four-necked flask with magnetic stirring under argon atmosphere. The mixture was degassed at 80 °C for 30 min to remove the air of the flask and then heated to the target temperature of 245 °C for 2 h. With the reaction proceeding, aliquots were derived from the hot mixture solution with a time interval of 30 min and immediately terminated the growth of GCIS BQDs in 1 mL of cyclohexane for subsequent measurement. The heat source was removed to make the solution cool to room temperature. A 4 mL portion of GCIS solution was taken out and purified by precipitation in excess ethanol and redispersed in trichloromethane for further characterization.

2.3. Synthesis of GCIS/ZnS Core/Shell BQDs. The GCIS solution were heated to 220 °C, and then Zn stock solution (110 mg of $Zn(OAc)_2{\cdot}2H_2O$ in 8 mL of ODE, 1 mL of OLA, and 1 mL of OA) was slowly added into the hot mixture solution in 4 batches with a time interval of 20 min. Aliquots were derived from the flask before injection of the next batch of Zn stock solution to monitor the process of reaction, especially the optical properties. In the end, excess ethanol was added, and the solution was centrifuged at 10 000 rpm for 10 min. The precipitations were redispersed in 3 mL of trichloromethane for further surface modification.

2.4. Synthesis of PEGylated Dextran-SA Polymeric Lipid Vesicles. DS was prepared according to the procedures reported previously.[26] Typically, dextran (3 g) was dissolved in 20 mL of DMSO, and SA (1 g) was dissolved in 30 mL of DMSO. Then, EDC·HCl (700 mg) was added into the SA solution. The above two solutions were mixed, and 100 mg of DMAP in 2 mL of DMSO was slowly added into the mixture solution. The reaction system was stirred overnight at room temperature. Excess ethanol was added to the reaction system, and the turbid mixture was centrifuged at 8000 rpm for 10 min. The obtained precipitate was resolved in 30 mL of DMSO and then dialyzed (MWCO: 3500 Da) against water for 48 h. Upon lyophilization, white powder was collected and stored in a dry place.

For synthesis of PEG-DS, PEG-COOH (100 mg) and DMAP (5 mg) were dissolved in 10 mL of DMSO. A 100 mg portion of DS was dissolved in 10 mL of DMSO and then added into the solution. After 12 h reaction at room temperature, the solution was dialyzed against pure water for 24 h. The PEG-DS powder was collected via lyophilization.

2.5. Phase Transfer of Hydrophobic GCIS/ZnS BQDs to the Aqueous Phase. The phase transfer procedure was implemented by adopting an ultrasonic emulsification method similar to that reported previously.[27,28] Briefly, PEG-DS (30 mg) was dissolved in 4 mL of deionized water in a 15 mL beaker, and then put under the ultrasonic cell disruptor (JY92-IID, Ningbo Scientz Biotechnology Co., LTD). A 400 μL portion of GCIS/ZnS QDs in dichloromethane was slowly dropped into the PEG-DS solution during the ultrasonication pulse

DOI: 10.1021/acsami.5b05372
ACS Appl. Mater. Interfaces 2015, 7, 18759−18768

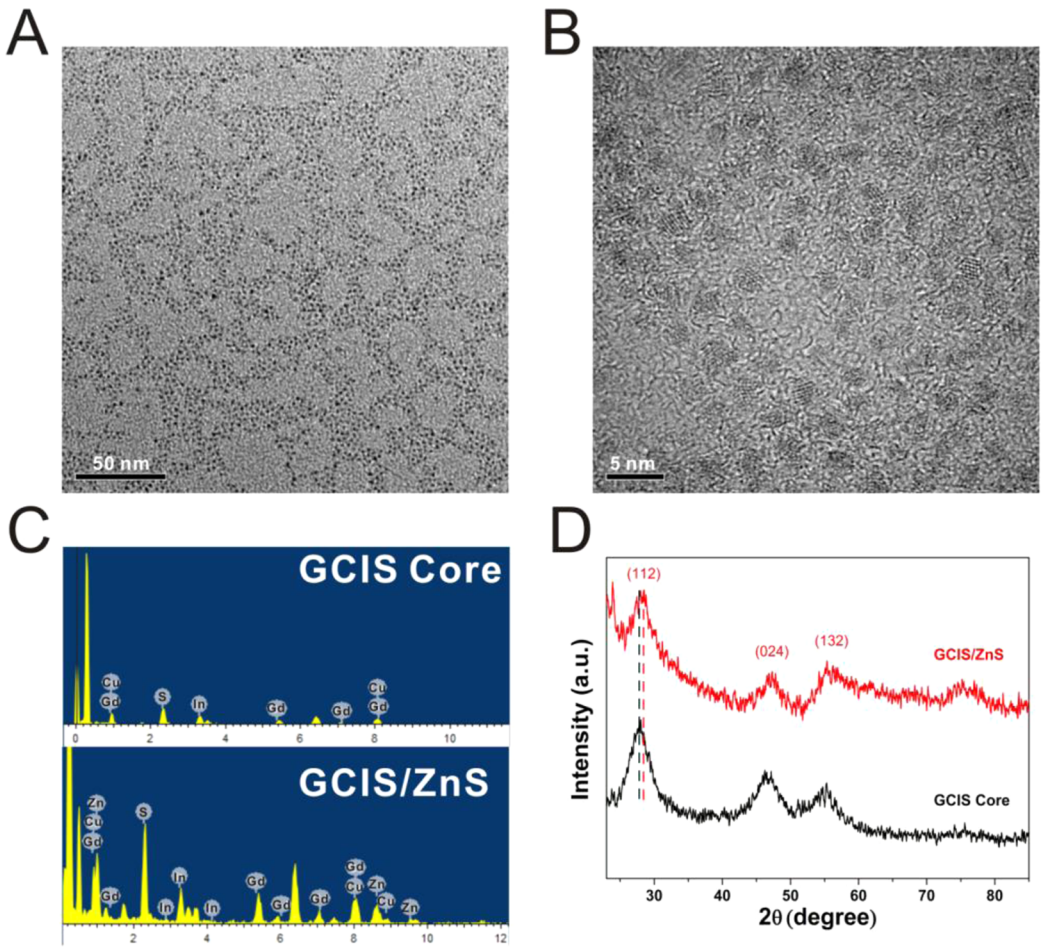

Figure 1. Representative HR-TEM images of GCIS/ZnS BQDs (A, B), and EDS spectra (C) and XRD patterns (D) of GCIS and GCIS/ZnS BQDs.

(200 W) for 5 s with interval of 3 s. The whole process lasted for 10 min. Upon the ultrasonication, the mixed emulsion was quickly transferred to a rotary evaporator to remove chloroform, resulting in a transparent aqueous solution containing GCIS/ZnS@PLVs. The resulting GCIS/ZnS@PLVs were purified and collected by centrifugation (45 000 rpm for 15 min). The obtained GCIS/ZnS@PLVs were finally redispersed in borate saline buffer (50 mM, pH = 8.2).

2.6. Materials Characterization. The morphology images of the as-prepared GCIS/ZnS BQDs were obtained by transmission electron microscopy (TEM) on a Tecnai G2 F20 instrument operated at an operating voltage of 200 kV. The hydrodynamic diameter (HD) and zeta potential of GCIS/ZnS@PLVs were measured by dynamic light-scattering (Nano ZS, Malvern). The powder X-ray diffraction (XRD) measurments were performed at room temperature by using a Rigaku Ultima III diffractometer equipped with a rotating anode and a Cu Ka radiation source. The UV−vis absorption and fluorescent emission spectra were recorded by Cary 50 spectrophotometer (Varian) and F-4500 spectrophotometer (Hitachi), respectively.

2.7. Colloidal Stability Studies. *2.7.1. HDs and Fluorescence Stability Test.* The obtained GCIS/ZnS@PLVs BQDs were mixed with various buffers at different pH value (3.5−12) and NaCl concentration (0−2 M). Similarly, we also investigated the stability profiles of the GCIS/ZnS@PLVs in the DMEM medium containing 10% fetal bovine serum (FBS) and 1% penicillin streptomycin (PS). Subsequently, the temporal evolution profiles of fluorescence and HDs were also monitored throughout the storage period up to 7 days.

2.7.2. Gd^{3+} Dissociation Test. GCIS/ZnS@PLV BQDs were dispersed into 3 mL of PBS (1×), and the Gd concentration in initial solution was measured first. After 1, 7, and 14 days, 1 mL of the initial solution was centrifuged by centrifugal filter units (10 K cutoff bf), respectively. The obtained filtrate without BQDs was measured by ICP-MS to determine the Gd concentration.

2.8. Relaxivity Characterization and MR Imaging *in Vitro*. The longitudinal (T_1) and transverse (T_2) relaxation times were measured with a 1.41 T minispec mq 60 NMR Analyzer (Bruker, Germany) at 37 °C. The MR images *in vitro* were acquired using a MicroMR-25 mini MR system (Niumag Corporation, Shanghai, China). The measurement parameters were as follows: T_1-weighted sequence, spin echo (SE), TR/TE = 500/18.2 ms, matrix acquisition = 90 × 90, NS = 2, FOV = 80 mm × 80 mm, slices = 1, slice width = 5.0 mm, slice gap = 0.55 mm, 0.55 T, 32.0 °C. Relaxivity values of r_1 and r_2 were calculated by fitting the $1/T_1$ and $1/T_2$ relaxation time (s^{-1}) versus Gd concentration (mM) curves.

2.9. *In Vitro* Cytotoxicity Assay. 3-(4,5-Dimethylthiazol-2-yl)-2, 5-diphenyltetrazolium bromide (MTT) assay was employed to analyze the *in vitro* cytotoxicity of the obtained GCIS/ZnS@PLVs. In brief, U87 cells were cultured in a 96-well plate with 6×10^3 cells per well. Subsequently, the cells were incubated in the culture medium for 24 h at 37 °C and 5% CO_2. The culture medium was discarded, and cells were incubated with complete medium containing 100 μL of GCIS/ZnS@PLVs at varied Cu concentration at 37 °C in the presence of 5% CO_2 for an additional 24 and 48 h, respectively. A 10 μL portion of MTT agentia (5 mg/mL) was added in the plates to replace the culture medium and then was incubated for an additional 4 h. Finally, 150 μL of dimethyl sulfoxide (DMSO) was added in each well, and the OD_{490} value (A) of each well, with background subtraction at 690 nm, was measured by a Tecan Infinite M200 monochromator-based multifunction microplate reader. The following formula was used to calculate the viability of cell growth: cell viability (%) = (mean of A value of treatment group/mean of A value of control) × 100%.

DOI: 10.1021/acsami.5b05372
ACS Appl. Mater. Interfaces 2015, 7, 18759−18768

2.10. Animal Model and Fluorescence/MR Tumor-Targeted *in Vivo* Imaging. All animal studies were conducted under a protocol approved by the Institutional Animal Care and Use Committee of Tongji University. For establishment of tumor models, 6×10^6 U87 cells suspended in 100 μL phosphate buffered saline (PBS) were subcutaneously injected into the right thigh of each mouse. For living imaging studies, nude mice (body weight *ca.* 23 g, $n = 3$) were anaesthetized by chloral hydrate (5%, 8 μL/g) via celiac injection before fluorescence/MR imaging were followed.

Fluorescence imaging was conducted on a Berthold NightOWL LB 983 *in vivo* Imaging System (Bad Wildbad, Germany). The excitation and emission filters were set as 530 and 780 nm, respectively, and images were captured by the CCD camera in a sequential acquisition mode. After 18 h, the nude mice were sacrificed and dissected to obtain the *ex vivo* fluorescence images of their main organs (heart, liver, spleen, lung, kidney) and tumor. Fluorescence intensity in the regions of interest (ROI) was calculated by using the Indigo software of *in vivo* Imaging System.

MR imaging was performed on a 1.5 T MR imaging system (GE Signa Excite), and images were acquired before, at subsequent intervals following intravenous injection (via the tail vein, 0.05 mmol Gd/kg) using a fat-saturated 3-D gradient echo imaging sequence. The detailed MR imaging parameters were set as follows: TR/TE = 300/18.2 ms, FOV = 40 mm × 40 mm, slices = 8, slice width = 2.5 mm, slice gap = 0.5 mm, flip angle = 90°. All imaging of postprocessing was performed using the Advantage Workstation 4.2 (AW4.2, General Electric Healthcare).

2.11. Histology Analysis. In order to evaluate the potential tissue damage, inflammation, or lesions GCIS/ZnS@PLVs caused, the major organs (heart, liver, spleen, lung, kidney, and intestine) were collected after intravenous injection 7 days, and then fixed with paraformaldehyde (4%), sliced, and stained with hematoxylin and eosin (H&E). Subsequently, the samples of organs were observed under an optical microscope.

3. RESULTS AND DISCUSSION

3.1. Morphology and Structural Characterization. As shown in Figure 1, the morphology and structure of the obtained GCIS/ZnS BQDs were investigated by TEM and XRD. Figure 1A,B revealed the GCIS/ZnS BQDs presented sphere structure with uniform size of 3.0 nm. The EDS element analysis results in Figure 1C and Table 1 confirmed that the

Table 1. Analysis of the Compositions of GCIS and GCIS/ZnS BQDs

	atomic composition (%)				
sample	Gd	Cu	In	Zn	S
GCIS	3.05	21.16	23.06	N.D.	52.73
GCIS/ZnS	2.65	16.28	17.60	10.65	53.82

GCIS BQDs were composed of Gd, Cu, In, and S with a molar ratio approaching 0.15:1:0.85:2. After ZnS coating, the stoichiometry ratio among of Gd, Cu, In, Zn, and S was 0.16:1:1:0.84:3. These demonstrated that Gd and Zn species were successfully introduced during the synthesis of GCIS/ZnS BQDs, while the Cu/In ratio has no obvious change after overcoating of the ZnS shell. The XRD patterns of GCIS and GCIS/ZnS were compared and displayed in Figure 1D. Both patterns consisted of three major peaks, indicating the cubic structure was well-maintained after ZnS coating. It is noticed that the diffraction peaks of GCIS/ZnS shifted toward higher angles compared with that of GCIS BQDs, which should be attributed to the smaller lattice constant of ZnS, suggesting the formation of ZnS around the GCIS.[29]

3.2. Optical and Magnetic Properties of the GCIS/ZnS BQDs. In this study, GCIS/ZnS BQDs were obtained with DDT as the sulfur source, surface ligand, and reaction solvent. Nevertheless, it is a great challenge to fabricate CuInS-based QDs with high qualities.[30] In our strategy, we set out to optimize the properties of the GCIS/ZnS BQDs by adjusting some reaction parameters, including reaction temperature, aging time, and the amount of Gd precursor.

As presented in Figure 2, the fluorescence property of GCIS/ZnS BQDs was a function of the reaction parameters, including reaction temperature, aging time, and the amount of Gd precursor. GCIS BQDs with higher PL intensity were synthesized at 245 °C (Figure 2A). Longer heating time was necessary to obtain bright GCIS BQDs at lower heating temperature (230 °C), while some aggregations were generated at elevated temperature 260 °C, which should be attributed to the over decomposition consumption of DDT. As depicted in Figure 2B, prolonging the heating aging time could contribute to stronger fluorescence intensity of GCIS BQDs, but has negligible effects on the fluorescence emission peaks. With aging time prolonging, surface defects could be greatly exhibited via Ostwald ripenng, which should accout for the time dependent fluorescence property. Although the introduced gadolinium as paramagnetic ions could have an adverse effect on the fluorescence property, we tried to exhibit it and achieve optimized fluorescence by varying the Gd precursor feeding ratio. As presented in Figure 2C, the brightest GCIS BQDs were fabricated when the Gd precursor was fixed at 0.1 mmol. Since CuInS-based BQDs exhibit a defect dependent PL emission related to copper deficiency, the existence of defect pairs of copper vacancies and other cations on Cu antisite contributes to the PL emission of CuInS-based BQDs following a donor−acceptor pair (DAP) recombination mechanism. The introduction of Gd species creates more defects and thus can potentially increase fluorescence, whereas the paramagnetic Gd species could also compromise the fluorescence. Therefore, the competitive balance was achieved at 0.1 mmol of Gd precursor, resulting in optimized fluorescence brightness. ZnS shell coating strategy was employed to enhance the fluorescence and photostability of obtained GCIS BQDs. As showed in Figure 2D, the overgrowth of ZnS resulted in a dramatic improvement of the PL intensity up to 8-fold enhancement, which typically led to a blue-shift of the PL spectrum, which was likely indicative of etching of the inner GCIS via cation exchange under shell growth conditions.[31,32] The time-resolved PL decay curves of GCIS and GCIS/ZnS are shown in Figure S1 (Supporting Information); obviously, after overcoating with ZnS shells, the contribution from the fast decay channel was reduced, and the lifetime was prolonged to some extent, from 256 to 310 ns (Table S1).

To evaluate the ability of GCIS/ZnS BQDs as an effective MR contrast agent, the longitudinal (T_1) and transverse (T_2) proton relaxation times were measured on a 1.5 T NMR analyzer. Prior to the measurement, the obtained hydrophobic GCIS/ZnS BQDs were transferred to aqueous phase with PEG-DS. As summarized in Figure 3, the GCIS/ZnS BQDs exhibited high r_1 value of 9.41 s^{-1} per mM of Gd, which was 3 times as much as that of Magnevist (Gd-DTPA), whose r_1 value was 3.56 mM^{-1} S^{-1} under the same measurement conditions. It has been demonstrated that the relaxivity ratio (r_2/r_1) is a crucial parameter to evaluate the efficiency of T_1 contrast agents; that is, low r_2/r_1 ratio less than 3.0 tends to produce a desired T_1 contrast effect. In this study, the GCIS/ZnS BQDs

DOI: 10.1021/acsami.5b05372
ACS Appl. Mater. Interfaces 2015, 7, 18759−18768

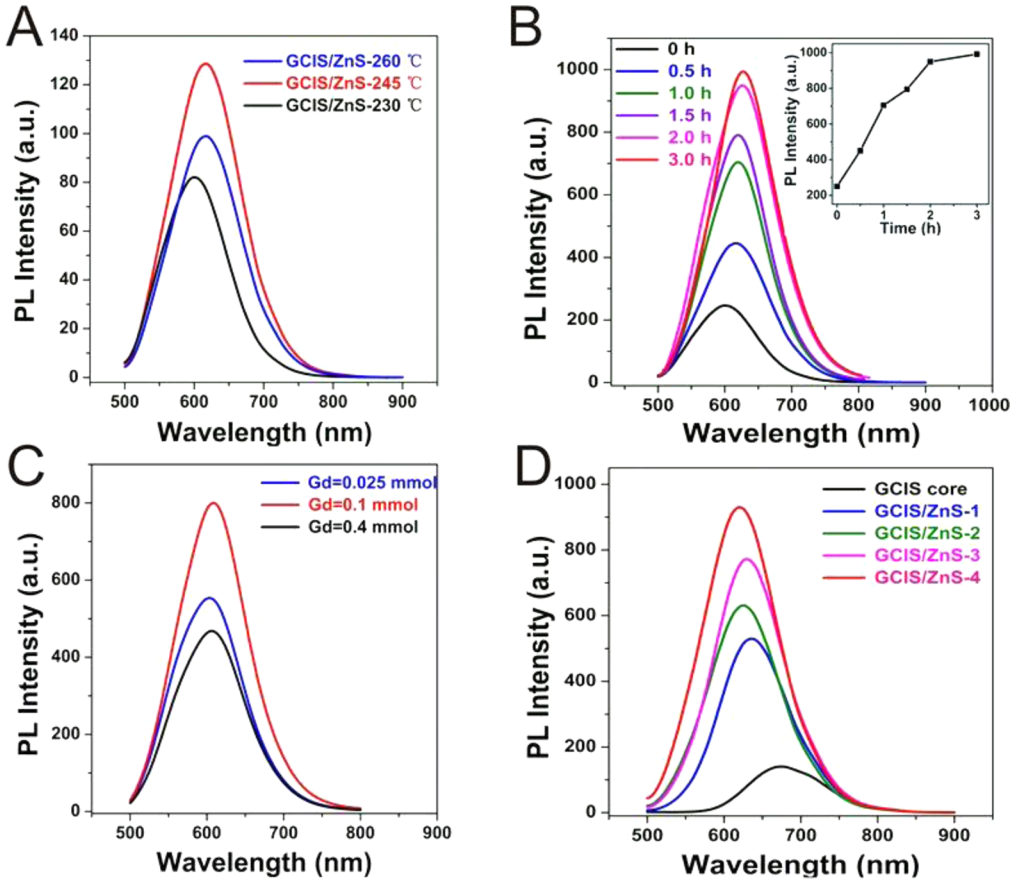

Figure 2. Optical properties of BQDs (wavelength, PL intensity) upon different experimental variables: (A) reaction temperature, (B) aging time, (C) the amount of Gd precursor, and (D) ZnS coating.

possessed a relatively low r_2/r_1 ratio of 1.4, suggesting that these GCIS/ZnS BQDs are efficient T_1 contrast agents.[33]

3.3. Stability of the GCIS/ZnS BQDs. Prior to the further biological applications, the obtained GCIS/ZnS BQDs were transferred to aqueous phase via polymer encapsulation strategy with our previously reported PEG-DS.[26] We have demonstrated that the PEG-DS consisting of dextran and stearyl acid possessed good biocompatibility. The GCIS/ZnS BQDs could be well-encapsulated into the PEG-DS PLVs via the hydrophobic interaction between the surface ligands DDT of GCIS/ZnS BQDs and stearyl acid segment of PEG-DS. As shown in Figure 4A,B, the TEM images (water/oil = 8/1) depicted that the GCIS/ZnS BQDs were densely assembled into the PEG-DS PLVs (~60 nm, Figure 4C), resulting in GCIS/ZnS@PLVs with good water dispersity. The zeta potential test result in Figure 4D revealed that the surface of the obtained GCIS/ZnS@PLVs were slightly negatively charged (−7.71 ± 2.48 mV), which suggested little protein adsorption onto the surface and implied potential good colloidal stability in biological fluid conditions. After phase transfer, it was found that the PL intensity can reserve more than 80% of the original emission intensity (Figure S2), accompanied by the wavelength being red-shifted about 35 nm, which may be attributed to the surface passivation of the QDs provided by the compact polymer layer and the interaction between the adjacent QDs encapsulated in each polymeric lipid vesicle.[34] The hydrodynamic diameters (HDs) of GCIS/ZnS@PLVs could be very tunable in the range 50−180 nm by varying the water/oil phase volume ratios (2/1, 4/1, and 8/1) for the ultrasonic emulsification, as shown in Figure S3.

The properties stability of the as-prepared GCIS/ZnS@PLVs were thoroughly investigated before their biological applications. Their HDs and fluorescence stability were evaluated by incubating the BQDs in diverse buffers with different pH and salt concentrations for 7 days. As summerized in Figure 5, the HDs of the GCIS/ZnS@PLVs stayed constant around 50 nm over the pH and salt concentrations ranges. Meanwhile, there's little change on the fluorescence intensity even after the torture conditions (Figure 5A,B). Subsequently, the GCIS/ZnS@PLVs were added into the DMEM solutions containing 10% FBS and 1% PS. Figure 5C,D revealed that the fluorescence intensity and HDs were well-maintained even after 48 h exposure. It has been demonstrated that the magnetic relaxivity was strongly dependent on the colloidal status of nanoparticles in aqueous phase.[35] The relaxivities of the GCIS/ZnS@PLVs in PBS (1×, pH 7.4) were continuously monitored over a period of 7 days. As displayed in Figure 5H, neither r_1 nor r_2/r_1 ratios showed obvious change throughout the incubation in PBS. From the ICP-MS measurement Gd^{3+} dissociation results in Table S2, there is no evidence for the detectable dissociation of gadolinium in the aqueous solution (leakage percentage <2%), which further implied the good structure stability of the obtained GCIS/ZnS@PLVs.

The above results suggested that the fabricated GCIS/ZnS@PLVs possessed qualified property stability, which paved the road for the further potential biological applications.

DOI: 10.1021/acsami.5b05372
ACS Appl. Mater. Interfaces 2015, 7, 18759−18768

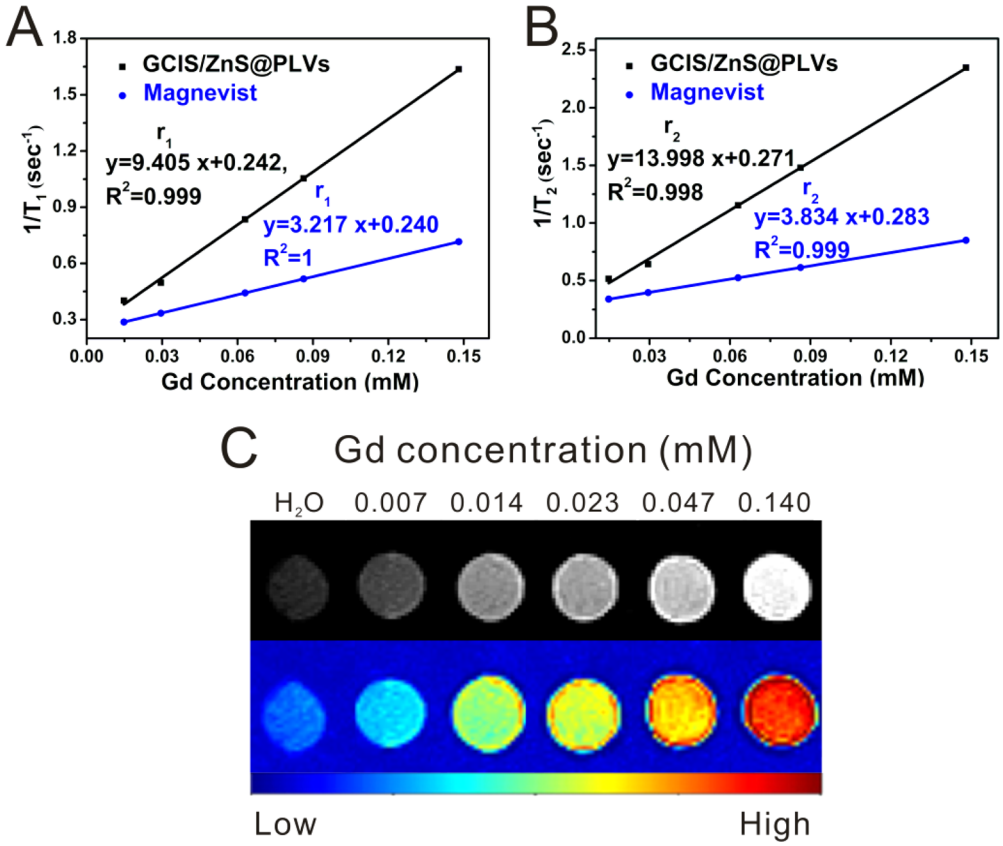

Figure 3. Magnetic properties of as-prepared GCIS/ZnS BQDs: (A) longitudinal rates ($1/T_1$, s^{-1}), (B) transverse rates ($1/T_2$, s^{-1}) of the GCIS/ZnS@PLVs and Magnevist as a function of the Gd concentration (mM); (C) T_1-weighted and the color-mapped of the GCIS/ZnS@PLVs with Gd concentrations ranging from 0.007 to 0.140 mM and H_2O.

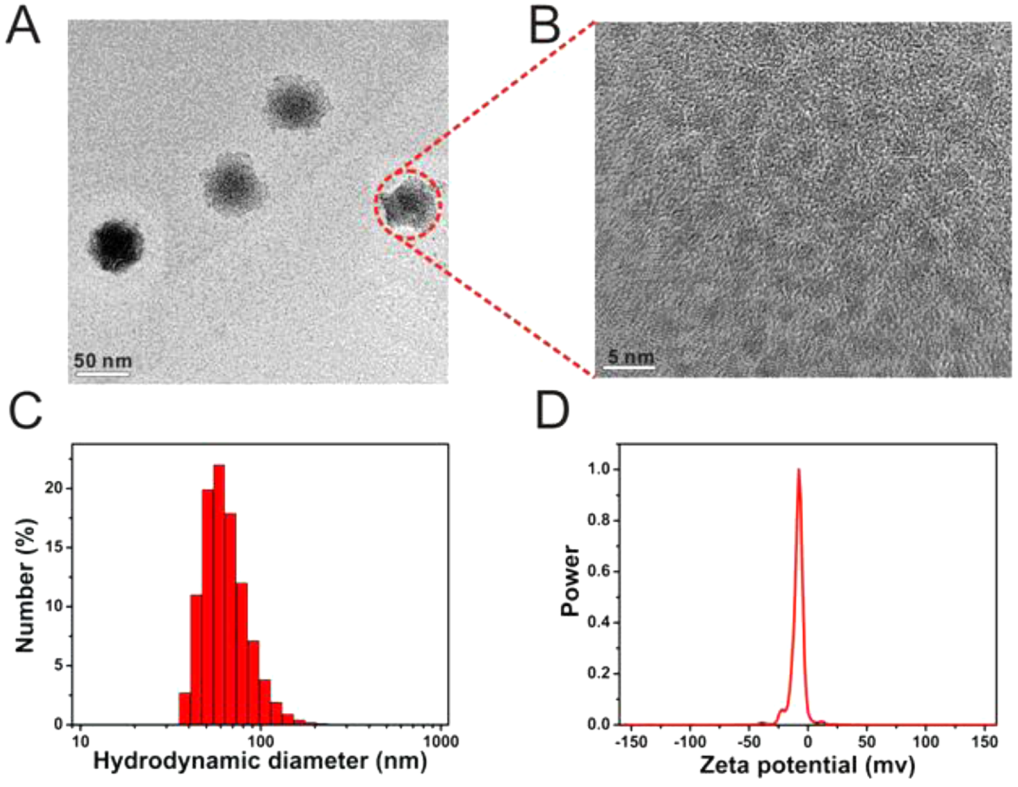

Figure 4. TEM (A, B), HDs (C), and zeta potential (D) of as-prepared hydrophilic GCIS/ZnS@PLVs BQDs.

DOI: 10.1021/acsami.5b05372
ACS Appl. Mater. Interfaces 2015, 7, 18759−18768

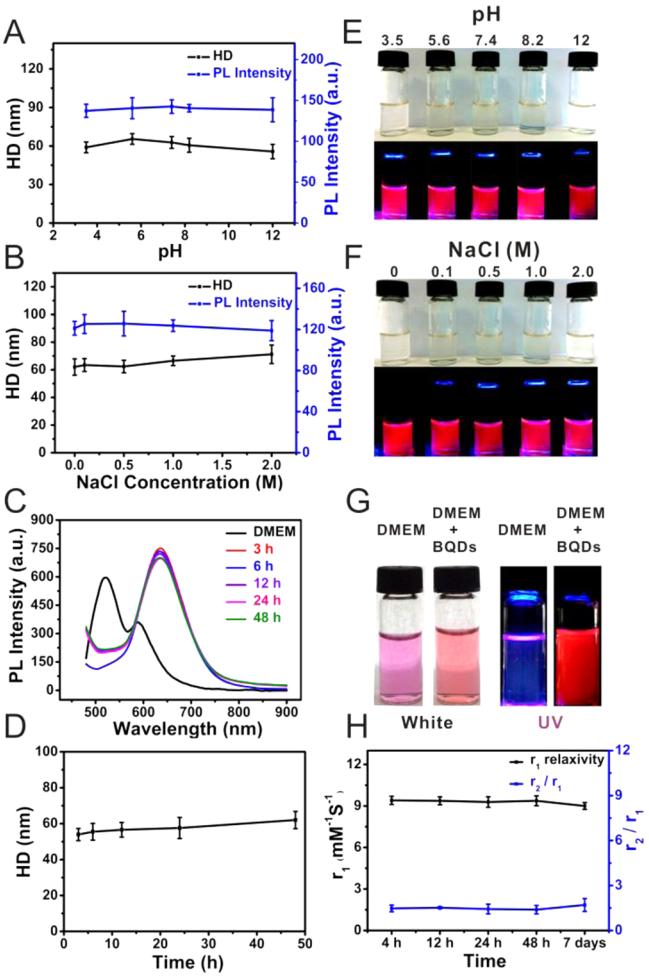

Figure 5. Colloidal stability of GCIS/ZnS@PLVs under different conditions, including (A) pH values, (B) ionic strengths, (C, D) DMEM, and (E, F, G) corresponding digital pictures. (H) Magnetic stability: change of r_1 relaxivity and r_2/r_1 ratio in PBS (1×, pH = 7.4) over a period of 7 days.

3.4. GCIS/ZnS BQDs for Tumor-Targeted Fluorescence/MR Dual-modal *in Vivo* Imaging. The cytotoxicity of GCIS/ZnS@PLVs was evaluated via MTT assay by incubating U87MG cells with GCIS/ZnS@PLVs at various concentrations of Cu for 24 and 48 h, respectively. The MTT results in Figure 6 indicated that the GCIS/ZnS BQDs showed little cytotoxicity against U87MG cells even at Cu concentrations up to 2.5 mM. Subsequently, the GCIS/ZnS BQDs were adopted for tumor-targeted *in vivo* imaging on the basis of enhanced permeability and retention (EPR) effect.[36−39]

The fluorescence imaging capability of GCIS/ZnS@PLVs was investigated to detect U87-expression in tumors. As shown in Figure 7A, a series of images were obtained at various time intervals (pre, 2, 4, 6, and 18 h). It was noticeable that the fluorescence signal derived from GCIS/ZnS@PLVs appeared in tumor and liver 4 h postinjection, possibly resulting from the enhanced accumulation of nanoparticles after circulation in the blood.[40,41] The light spots in the brain area may most likely be the enhanced plicated skins, as optical imaging is always sensitive to the autofluorescence of tissues, hairs, and feeding food of mice. Subsequently, fluorescence signals nearly vanished after 18 h postinjection, which indicates most BQDs are cleared gradually from the body. As pharmacodynamics of

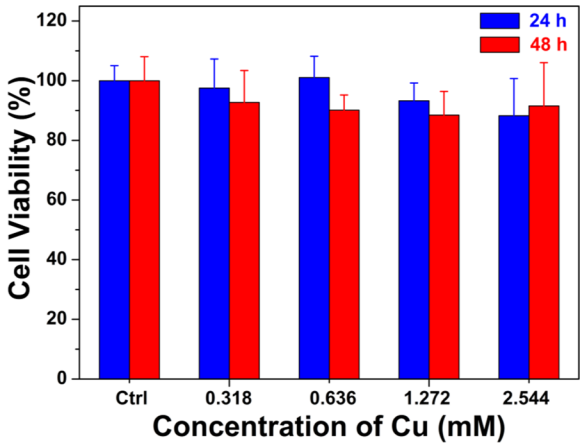

Figure 6. *In vitro* cytotoxicity of the GCIS/ZnS@PLVs against U87 cells following 24 and 48 h.

nanoparticles at the tumor is different from that of surrounding tissues, this time dependent *in vivo* imaging of GCIS/ZnS@PLVs can monitore and confirm the suspect tumor. *Ex vivo* fluorescence images (Figure 7B) and regions of interest (ROI) measurement results (Figure 7D) further verified the conspicuous fluorescence signal from the tumor, although the fluorescence intensity of liver was highest among all the organs, owing to the macrophage uptake of nanoparticles. A relatively lower uptake of BQDs in the kidney may be attributed to the existing single encapsulation of BQDs into one polymeric lipid vesicle, resulting in the uptake of kidney. Also, liver degradation of GCIS/ZnS@PLVs can lead to small nanoparticles in kidneys.

The MR imaging studies were carried out on a 1.5 T MR imaging system. T_1-weighted MR transverse images were acquired preinjection, and 2, 4, 6, and 18 h postinjection GCIS/ZnS@PLVs (Figure 7C), at a dosage of 0.05 mmol Gd/kg body weight of nude mice. The first image was taken and regarded as the baseline for comparison, and no obvious changes were found in T_1-weighted MR image of tumor at 2 h postinjection, which was effectively due to little accumulation of the BQDs around the tumor site. Nevertheless, a significant contrast enhancement in T_1-weighted MR image was clearly visible in the tumor site at 4 h postinjection. This time dependent accumulation in the tumor is most possibly attributed to the EPR effect.[42,43] The enhanced-MRI capability of BQDs 6 and 18 h postinjection decreased gradually. Data analysis of the relative signal intensities shows the tumor was enhanced by 11.1%, 73.8%, 63%, and 30% at 2, 4, 6, and 18 h postinjection, respectively (Figure 7E). As a control, we performed the *in vivo* T_1-weighted imaging on tumor-bearing mice injected with Magnevist (commercial contrast agent). Images at various postinjection time points were presented in Figure S4 (Supporting Information). It is demonstrated that Gd-DTPA exhibited much lower imaging intensity compared with the GCIS/ZnS BQDs at the tumor. Data analysis of the relative signal intensities shows the tumor was enhanced by 29.4%, 10%, 7%, and 4% at 2, 4, 6, and 18 h, respectively. Gd-DTPA, a small molecule, has short circulation time in the body. This fast clearance results in a limited imaging time window for technicians. The low molecule weight of Gd-DTPA can also lead to an inconspicuous EPR effect. These two unfavorable conditions hinder the accumulation of Gd-DTPA at the tumor. Considering proper molecule weight, high stability, and potent

DOI: 10.1021/acsami.5b05372
ACS Appl. Mater. Interfaces 2015, 7, 18759−18768

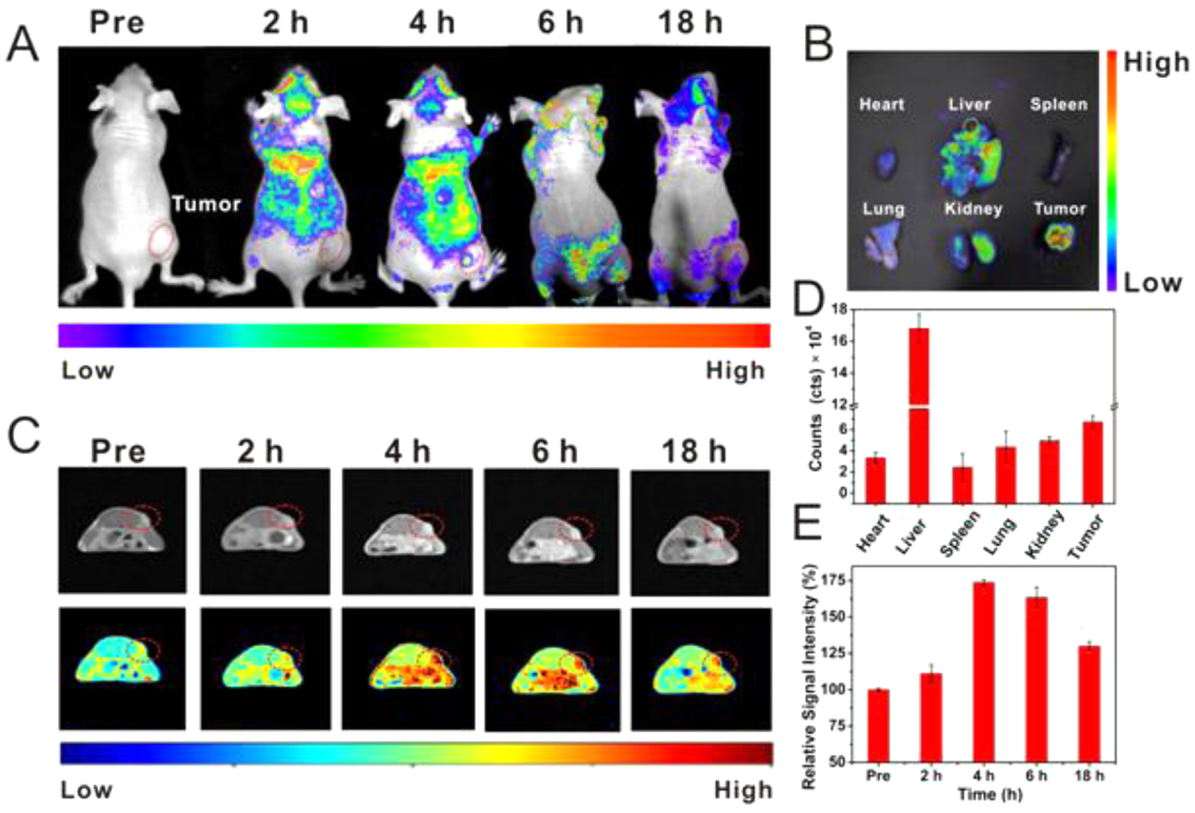

Figure 7. *In vivo* fluorescence imaging (A), *ex vivo* imaging (B), and T_1-weighted imaging (C) (18 h postinjection) of U87 tumor-bearing mice (red circles) after tail-vein injection of GCIS/ZnS@PLVs. ROI fluorescence analysis of dissected organs (heart, liver, spleen, lung, kidney) and tumor at 18 h postinjection of GCIS/ZnS@PLVs (D). Relative T_1 signal enhancement values of the tumor before and after injection of GCIS/ZnS@PLVs (E).

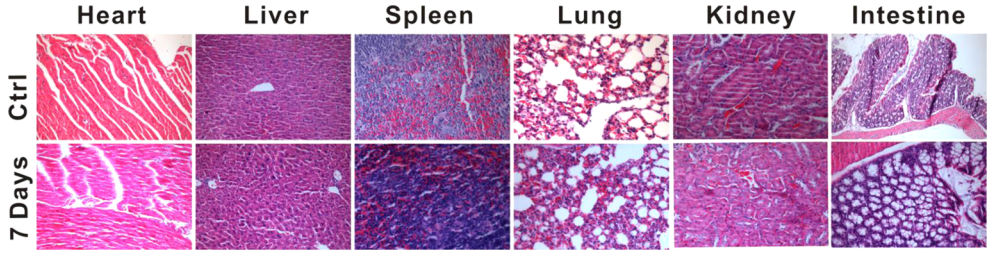

Figure 8. H&E stained images of major organs (heart, liver, spleen, lung, kidney, intestine) of the mice collected from control and 7 days after intravenous injection of GCIS/ZnS@PLVs.

MRI enhancement, GCIS/ZnS@PLVs present an effective T_1-weighted MR contrast agent *in vivo*.

The *in vivo* toxicity of the fabricated Cd-freed GCIS/ZnS@PLVs BQDs was investigated by an H&E staining examination. Several major susceptible organs, such as heart, liver, spleen, lung, kidney, and intestine, were collected to examine the damage of tissues. The tissue structures of major organs from mice postinjection of GCIS/ZnS@PLVs BQDs were almost intact. No necrosis and inflammatory infiltrate were observed after 7 days postinjection (Figure 8). It can be inferred that the fabricated Cd-freed GCIS/ZnS@PLVs BQDs were biocompatible at the tested dose, which is crucial for *in vivo* biomedical applications.

4. CONCLUSIONS

In summary, a facile one-pot synthetic strategy was put forward to prepare Gd-doped Cd-free CuInS/ZnS fluorescence/MR bimodal nanoprobes with the advantages of optimized properties. At optimized reaction conditions, GCIS/ZnS BQDs were obtained with balanced fluorescence/MR porperties, and the balanced point was realized at Cu/In/Gd = 1/1/0.5, temperature = 245 °C, aging time = 2 h, and ZnS coating. After surface modification with PEG-DS, the obtained GCIS/ZnS@PLVs exhibited pronounced near-infrared fluorescence (emission wavelength: 670 nm) as well as high longitudinal relaxivity (r_1 = 9.45 mM^{-1} S^{-1}) in water with good colloidal stability. The subsequent animal experimental results confirmed GCIS/ZnS@PLVs can realize the tumor-targeted fluorescence/MR dual-modal *in vivo* imaging and act as a kind of qualified bimodal contrast agent. This reported strategy and as-prepared GCIS/ZnS@PLVs nanoprobes provide a new pathway to explore further applications of nanoprobes with robust performance for tumor diagnosis in the future.

DOI: 10.1021/acsami.5b05372
ACS Appl. Mater. Interfaces 2015, 7, 18759−18768

■ ASSOCIATED CONTENT

Supporting Information

The Supporting Information is available free of charge on the ACS Publications website at DOI: 10.1021/acsami.5b05372.

Additional tables and figures including fitting parameters, PL data, hydrodynamic diameter data, Gd concentrations, and tumor imaging (PDF)

■ AUTHOR INFORMATION

Corresponding Authors

*E-mail: bingbozhang@tongji.edu.cn. Phone: +86-21-65983706-805.

*E-mail: jinchang@tju.edu.cn. Phone: +86-22-27401821.

Author Contributions

Weitao Yang and Weisheng Guo contributed equally.

Notes

The authors declare no competing financial interest.

■ ACKNOWLEDGMENTS

This work was supported by the National Natural Science Foundation of China (51373117, 51303126, 81371618, 81271629), Key Project of Tianjin Natural Science Foundation (13JCZDJC33200), National High Technology Program of China (2012AA022603), the Doctoral Base Foundation of Educational Ministry of China (20120032110027), Shanghai Innovation Program (14ZZ039), Program for Outstanding Young Teachers in Tongji University, and the Fundamental Research Funds for the Central Universities.

■ REFERENCES

(1) Terreno, E.; Delli Castelli, D.; Viale, A.; Aime, S. Challenges for Molecular Magnetic Resonance Imaging. *Chem. Rev.* **2010**, *110*, 3019−3042.

(2) Cheon, J.; Lee, J. H. Synergistically Integrated Nanoparticles as Multimodal Probes for Nanobiotechnology. *Acc. Chem. Res.* **2008**, *41*, 1630−1640.

(3) Weissleder, R.; Pittet, M. J. Imaging in the era of Molecular Oncology. *Nature* **2008**, *452*, 580−589.

(4) Caravan, P. Strategies for Increasing the Sensitivity of Gadolinium Based MRI Contrast Agents. *Chem. Soc. Rev.* **2006**, *35*, 512−523.

(5) Smith, A. M.; Nie, S. M. Next-Generation Quantum Dots. *Nat. Biotechnol.* **2009**, *27*, 732−733.

(6) Zheng, C. F.; Zheng, M. B.; Gong, P.; Jia, D. X.; Zhang, P. F.; Shi, B. H.; Sheng, Z. H.; Ma, Y. F.; Cai, L. T. Indocyanine Green-Loaded Biodegradable Tumor Targeting Nanoprobes for In Vitro and In Vivo Imaging. *Biomaterials* **2012**, *33* (22), 5603−5609.

(7) Yu, K.; Schanze, K. S. Preface: Forum on Biomedical Applications of Colloidal Photoluminescent Quantum Dots. *ACS Appl. Mater. Interfaces* **2013**, *5* (8), 2785−2785.

(8) Kairdolf, B. A.; Smith, A. M.; Stokes, T. H.; Wang, M. D.; Young, A. N.; Nie, S. M. Semiconductor Quantum Dots for Bioimaging and Biodiagnostic Applications. *Annu. Rev. Anal. Chem.* **2013**, *6*, 143−162.

(9) Shao, L. J.; Gao, Y. F.; Yan, F. Semiconductor Quantum Dots for Biomedicial Applications. *Sensors* **2011**, *11*, 11736−11751.

(10) Liu, Y. L.; Ai, K. L.; Yuan, Q. H.; Lu, L. H. Fluorescence-Enhanced Gadolinium-Doped Zinc Oxide Quantum Dots for Magnetic Resonance and Fluorescence Imaging. *Biomaterials* **2011**, *32*, 1185−1192.

(11) Norris, D. J.; Efros, A. L.; Erwin, S. C. Doped nanocrystals. *Science* **2008**, *319*, 1776−1779.

(12) Erwin, S. C.; Zu, L. J.; Haftel, M. I.; Efros, A. L.; Kennedy, T. A.; Norris, D. J. Doping Semiconductor Nanocrystals. *Nature* **2005**, *436*, 91−94.

(13) Wang, S.; Jarrett, B. R.; Kauzlarich, S. M.; Louie, A. Y. Core/Shell Quantum Dots with High Relaxivity and Photoluminescence for Multimodality Imaging. *J. Am. Chem. Soc.* **2007**, *129*, 3848−3856.

(14) Zhang, F.; Sun, T. T.; Zhang, Y.; Li, Q.; Chai, C.; Lu, L.; Shen, W.; Yang, J.; He, X. W.; Zhang, Y. K.; Li, W. Y. Facile Synthesis of Functional Gadolinium-doped CdTe Quantum Dots for Tumor-targeted Fluorescence and Magnetic Resonance Dual-Modality Imaging. *J. Mater. Chem. B* **2014**, *2*, 7201−7209.

(15) Yu, K.; Ng, P.; Ouyang, J. Y.; Zaman, M. B.; Abulrob, A.; Baral, T. N.; Fatehi, D.; Jakubek, Z. J.; Kingston, D.; Wu, X. H.; Liu, X. Y.; Hebert, C.; Leek, D. M.; Whitfield, D. M. Low-Temperature Approach to Highly Emissive Copper Indium Sulfide Colloidal Nanocrystals and Their Bioimaging Applications. *ACS Appl. Mater. Interfaces* **2013**, *5*, 2870−2880.

(16) Li, L.; Daou, T. J.; Texier, I.; Tran, T. K. C.; Nguyen, Q. L.; Reiss, P. Highly Luminescent CuInS2/ZnS Core/Shell Nanocrystals: Cadmium-Free Quantum Dots for In Vivo Imaging. *Chem. Mater.* **2009**, *21*, 2422−2429.

(17) Chen, B. K.; Zhong, H. Z.; Zhang, W. Q.; Tan, Z. A.; Li, Y. F.; Yu, C. R.; Zhai, T. Y.; Bando, Y. S.; Yang, S. Y.; Zou, B. S. Highly Emissive and Color-Tunable CuInS2-Based Colloidal Semiconductor Nanocrystals: Off-Stoichiometry Effects and Improved Electroluminescence Performance. *Adv. Funct. Mater.* **2012**, *22*, 2081−2088.

(18) Guo, W. S.; Yang, W. T.; Wang, Y.; S un, X. L.; Liu, Z. Y.; Zhang, B. B.; Chang, J.; Chen, X. Y. Color-Tunable Gd-Zn-Cu-In-S/ZnS Quantum Dots for Dual Modality Magnetic Resonance and Fluorescence Imaging. *Nano Res.* **2014**, *7*, 1581−1591.

(19) Guo, W. S.; Sun, X. L.; Jacobson, O.; Yan, X. F.; Min, K.; Srivatsan, A.; Niu, G.; Kiesewetter, D. O.; Chang, J.; Chen, X. Y. Intrinsically Radioactive Cu-64 CuInS/ZnS Quantum Dots for PET and Optical Imaging: Improved Radiochemical Stability and Controllable Cerenkov Luminescence. *ACS Nano* **2015**, *9* (1), 488−495.

(20) Xing, X. H.; Zhang, B. B.; Wang, X. H.; Liu, F. J.; Shi, D. L.; Cheng, Y. S. An ″Imaging-biopsy″ Strategy for Colorectal Tumor Reconfirmation by Multipurpose Paramagnetic Quantum Dots. *Biomaterials* **2015**, *48*, 16−25.

(21) Zhang, B. B.; Gong, X. Q.; Li, Z. Q.; Guo, F. F.; Cai, S. Y.; Kong, J. L.; Yang, Q. H.; Ma, H.; Chang, J.; Shi, D. L. Preparation of Gd-III/Quantum Dots Multimodal Imaging Probes for Disease Diagnosis. *Chem. J. Chin. U* **2010**, *31*, 982−985.

(22) Li, L. A.; Pandey, A.; Werder, D. J.; Khanal, B. P.; Pietryga, J. M.; Klimov, V. I. Efficient Synthesis of Highly Luminescent Copper Indium Sulfide-Based Core/Shell Nanocrystals with Surprisingly Long-Lived Emission. *J. Am. Chem. Soc.* **2011**, *133*, 1176−1179.

(23) Deng, D. W.; Chen, Y. Q.; Cao, J.; Tian, J. M.; Qian, Z. Y.; Achilefu, S.; Gu, Y. Q. High-Quality CuInS2/ZnS Quantum Dots for In vitro and In vivo Bioimaging. *Chem. Mater.* **2012**, *24*, 3029−3037.

(24) Zhong, H. Z.; Bai, Z. L.; Zou, B. S. Tuning the Luminescence Properties of Colloidal I-III-VI Semiconductor Nanocrystals for Optoelectronics and Biotechnology Applications. *J. Phys. Chem. Lett.* **2012**, *3*, 3167−3175.

(25) Li, L. A.; Pandey, A.; Werder, D. J.; Khanal, B. P.; Pietryga, J. M.; Klimov, V. I. Efficient Synthesis of Highly Luminescent Copper Indium Sulfide-Based Core/Shell Nanocrystals with Surprisingly Long-Lived Emission. *J. Am. Chem. Soc.* **2011**, *133*, 1176−1179.

(26) Wang, S.; Wang, H. J.; Liu, Z. Y.; Wang, L. L.; Wang, X. M.; Su, L.; Chang, J. Smart pH- and Reduction-dual-responsive Folate-PEG-coated Polymeric Lipid Vesicles for Tumor-triggered Targeted Drug Delivery. *Nanoscale* **2014**, *6*, 7635−7642.

(27) Zhang, B. B.; Li, Q.; Yin, P. H.; Rui, Y. P.; Qiu, Y. Y.; Wang, Y.; Shi, D. L. Ultrasound-Triggered BSA/SPION Hybrid Nanoclusters for Liver-Specific Magnetic Resonance Imaging. *ACS Appl. Mater. Interfaces* **2012**, *4*, 6479−6486.

(28) Zhang, B. B.; Wang, X. H.; Liu, F. J.; Cheng, Y. S.; Shi, D. L. Effective Reduction of Nonspecific Binding by Surface Engineering of Quantum Dots with Bovine Serum Albumin for Cell-Targeted Imaging. *Langmuir* **2012**, *28*, 16605−16613.

(29) Zhang, W. J.; Lou, Q.; Ji, W. Y.; Zhao, J. L.; Zhong, X. H. Color-Tunable Highly Bright Photoluminescence of Cadmium-Free Cu-

DOI: 10.1021/acsami.5b05372
ACS Appl. Mater. Interfaces 2015, 7, 18759−18768

Doped Zn-In-S Nanocrystals and Electroluminescence. *Chem. Mater.* **2014**, *26*, 1204−1212.
(30) Xie, R. G.; Rutherford, M.; Peng, X. G. Formation of High-Quality I-III-VI Semiconductor Nanocrystals by Tuning Relative Reactivity of Cationic Precursors. *J. Am. Chem. Soc.* **2009**, *131*, 5691−5697.
(31) Park, J.; Kim, S. W. CuInS2/ZnS Core/Shell Quantum Dots by Cation Exchange and Their Blue-Shifted Photoluminescence. *J. Mater. Chem.* **2011**, *21*, 3745−3750.
(32) Guo, W. S.; Chen, N.; Tu, Y.; Dong, C. H.; Zhang, B. B.; Hu, C. H.; Chang, J. Synthesis of Zn-Cu-In-S/ZnS Core/Shell Quantum Dots with Inhibited Blue-Shift Photoluminescence and Applications for Tumor Targeted Bioimaging. *Theranostics* **2013**, *3*, 99−108.
(33) Caravan, P.; Ellison, J. J.; McMurry, T. J.; Lauffer, R. B. Gadolinium(III) Chelates as MRI Contrast Agents: Structure, Dynamics, and Applications. *Chem. Rev.* **1999**, *99*, 2293−2352.
(34) Dong, C. H.; Liu, Z. Y.; Zhang, L.; Guo, W. S.; Li, X.; Liu, J. Q.; Wang, H. J.; Chang, J. pHe-Induced Charge-Reversible NIR Fluorescence Nanoprobe for Tumor-Specific Imaging. *ACS Appl. Mater. Interfaces* **2015**, *7*, 7566−7575.
(35) Liang, G. H.; Ye, D. X.; Zhang, X. X.; Dong, F.; Chen, H.; Zhang, S.; Li, J. Q.; Shen, X. R.; Kong, J. L. One-Pot Synthesis of Gd3+-Functionalized Gold Nanoclusters for Dual Model (Fluorescence/Magnetic Resonance) Imaging. *J. Mater. Chem. B* **2013**, *1*, 3545−3552.
(36) Ding, K.; Jing, L. H.; Liu, C. Y.; Hou, Y.; Gao, M. Y. Magnetically Engineered Cd-free Quantum Dots as Dual-Modality Probes for Fluorescence/Magnetic Resonance Imaging of Tumors. *Biomaterials* **2014**, *35*, 1608−1617.
(37) Liu, J. B.; Yu, M. X.; Zhou, C.; Yang, S. Y.; Ning, X. H.; Zheng, J. Passive Tumor Targeting of Renal-Clearable Luminescent Gold Nanoparticles: Long Tumor Retention and Fast Normal Tissue Clearance. *J. Am. Chem. Soc.* **2013**, *135*, 4978−4981.
(38) Robinson, J. T.; Hong, G. S.; Liang, Y. Y.; Zhang, B.; Yaghi, O. K.; Dai, H. J. In Vivo Fluorescence Imaging in the Second Near-Infrared Window with Long Circulating Carbon Nanotubes Capable of Ultrahigh Tumor Uptake. *J. Am. Chem. Soc.* **2012**, *134*, 10664−10669.
(39) Iyer, A. K.; Khaled, G.; Fang, J.; Maeda, H. Exploiting the Enhanced Permeability and Retention Effect for Tumor Targeting. *Drug Discovery Today* **2006**, *11*, 812−818.
(40) Yang, H.; Mao, H.; Wan, Z.; Zhu, A.; Guo, M.; Li, Y.; Li, X.; Wan, J.; Yang, X.; Shuai, X. Micelles Assembled with Carbocyanine Dyes for Theranostic Near-Infrared Fluorescent Cancer Imaging and Photothermal Therapy. *Biomaterials* **2013**, *34*, 9124−9133.
(41) Wang, Y.; Yang, T.; Ke, H.; Zhu, A.; Wang, Y.; Wang, J.; Shen, J.; Liu, G.; Chen, C.; Zhao, Y. Smart Albumin-Biomineralized Nanocomposites for Multimodal Imaging and Photothermal Tumor Ablation. *Adv. Mater.* **2015**, *27*, 3874.
(42) Le Duc, G.; Miladi, I.; Alric, C.; Mowat, P.; Brauer-Krisch, E.; Bouchet, A.; Khalil, E.; Billotey, C.; Janier, M.; Lux, F.; Epicier, T.; Perriat, P.; Roux, S.; Tillement, O. Toward an Image-Guided Microbeam Radiation Therapy Using Gadolinium-Based Nanoparticles. *ACS Nano* **2011**, *5*, 9566−9574.
(43) Ni, D. L.; Bu, W. B.; Zhang, S. J.; Zheng, X. P.; Li, M.; Xing, H. Y.; Xiao, Q. F.; Liu, Y. Y.; Hua, Y. Q.; Zhou, L. P.; Peng, W. J.; Zhao, K. L.; Shi, J. L. Single Ho3+-Doped Upconversion Nanoparticles for High-Performance T-2-Weighted Brain Tumor Diagnosis and MR/UCL/CT Multimodal Imaging. *Adv. Funct. Mater.* **2014**, *24*, 6613−6620.

DOI: 10.1021/acsami.5b05372
ACS Appl. Mater. Interfaces 2015, 7, 18759−18768